

Environmental stability and anisotropic resistivity of Co-doped $\text{Na}_{1-\delta}\text{Fe}_{1-x}\text{Co}_x\text{As}$ N. Spyrisson,^{1,2} M. A. Tanatar,^{1,2,*} Kyuil Cho,^{1,2} Y. Song,³ Pengcheng Dai,³ Chenglin Zhang,³ and R. Prozorov^{1,2,†}¹*Department of Physics and Astronomy, Iowa State University, Ames, Iowa 50011, USA*²*The Ames Laboratory, Ames, Iowa 50011, USA*³*Department of Physics and Astronomy, The University of Tennessee, Knoxville, Tennessee 37996-1200, USA*

(Received 17 August 2012; revised manuscript received 10 October 2012; published 23 October 2012)

Temperature-dependent resistivity is studied in single crystals of iron-arsenide superconductor $\text{Na}_{1-\delta}\text{Fe}_{1-x}\text{Co}_x\text{As}$ for electrical current directions along, $\rho_a(T)$, and transverse, $\rho_c(T)$, to the Fe-As layers. Doping with Co increases stability of this compound to reaction with the environment and suppresses numerous features in both $\rho_a(T)$ and $\rho_c(T)$ compared to the stoichiometric NaFeAs . Evolution of $\rho_a(T)$ with x follows a universal trend observed in other pnictide superconductors, exhibiting a T -linear temperature dependence close to the optimal doping and development of T^2 dependence upon further doping. $\rho_c(T)$ in parent compound shows a nonmonotonic behavior with a crossover from nonmetallic resistivity increase on cooling from room temperature down to ~ 80 K to a metallic decrease below this temperature. Both $\rho_a(T)$ and $\rho_c(T)$ show several correlated crossoverlike features at $T > 80$ K. Despite a general trend towards more metallic behavior of interplane resistivity in Co-doped samples, the temperature of the crossover from insulating to metallic behavior (80 K) does not change much with doping.

DOI: [10.1103/PhysRevB.86.144528](https://doi.org/10.1103/PhysRevB.86.144528)

PACS number(s): 74.70.Dd, 72.15.-v, 74.25.Jb

I. INTRODUCTION

Structurally, iron based superconductors are layered materials, in which the FeAs (or iron chalcogenide) layer is the main building block for a variety of compounds.¹⁻³ Since the dominant contribution to the density of states at the Fermi level comes from the iron $3d$ orbitals, one can expect a significant electronic anisotropy of the compounds revealed in the in-plane and out-of-plane transport. Contrary to this expectation, the most studied families of iron arsenides, those based on BaFe_2As_2 , have rather low anisotropy ratio $\gamma_\rho \equiv \rho_c/\rho_a \sim 4$ at T_c .⁴ In transition-metal-doped $\text{Ba}(\text{Fe}_{1-x}\text{M}_x)_2\text{As}_2$ ($M = \text{Co}, \text{Ni}, \text{Rh}, \text{Pd}, \text{BaM122}$ in the following), $\rho_c(T)$ also shows a very different temperature dependence compared with $\rho_a(T)$, revealing a broad crossover from nonmetallic to metallic temperature dependence assigned in our systematic doping studies to the formation of a pseudogap.⁴⁻⁷

Another interesting feature of iron arsenides that distinguishes them from the copper oxide based (cuprate) superconductors⁸ is a strong variation of the functional form of temperature-dependent resistivity for various types and levels of dopings. The general trend of $\rho_a(T)$ evolution is the presence of a T -linear region immediately above T_c for optimally doped compositions.⁹⁻¹² At higher temperatures this T -linear behavior, for example, in hole-doped $\text{Ba}_{1-x}\text{K}_x\text{Fe}_2\text{As}_2$ and in self-doped $\text{Na}_{1-\delta}\text{FeAs}$, is terminated by the pseudogap.^{12,13}

Systematic studies of the temperature-dependent electrical resistivity are very important for the general understanding of superconductivity in this family of materials. Scattering in the normal state in the vicinity of the magnetic quantum critical point leads to the characteristic T -linear temperature dependence of $\rho_a(T)$, which then evolves towards Fermi-liquid T^2 -behavior with doping (see Ref. 14 for a review). Deviations from this general behavior provide an insight into electronic and magnetic correlations,¹⁵ in particular, into the mechanism of nematic state formation.¹⁶⁻¹⁸

In this paper we report the systematics of doping evolution of in-plane and interplane resistivity of electron-doped

$\text{Na}_{1-\delta}\text{Fe}_{1-x}\text{Co}_x\text{As}$. This compound shows a “domelike” phase diagram which is very similar to BaCo122 .^{12,19,20} As such, this study brings additional insight into the scattering and correlation phenomena of the ironbased superconductors.

II. EXPERIMENT

Magnetic characterization of the samples was performed using radiofrequency (14 MHz) ac susceptibility measurements with a tunnel-diode resonator (TDR).^{21,22} Briefly, TDR is a self-oscillating LC tank circuit powered by a properly biased tunnel diode. The sample is mounted with Apiezon N grease on a sapphire rod and is inserted in the inductor (coil). The sample temperature is controlled independent of the resonant circuit, which is actively stabilized at the constant temperature. The measured frequency shift is proportional to the differential magnetic susceptibility of the sample.²² In this work, for quick mounting and measurement protocols we used a simplified version of the TDR susceptometer (a “dipper”), which is inserted directly into a transport ⁴He dewar and gives a very quick turnaround measurement time of typically 30 min per sample. The tradeoff of this quick measurement protocol is reduced stability and higher temperature-dependent background as compared to our high-stability ³He and dilution refrigerator versions of the TDR susceptometer. Nevertheless, the dipper is perfectly suitable to study magnetic signature of the superconducting transition.

Single crystals of $\text{Na}(\text{Fe}_{1-x}\text{Co}_x)\text{As}$ with $x = 0, 0.025, 0.05, 0.08, \text{ and } 0.10$ were synthesized by sealing a mixture of Na, Fe, As, and Co together in Ta tubes and heating it to 950 °C, followed by 5 °C/h cooling down to 900 °C.²³ The x in samples was defined as the nominal ratio, which gives some variation with electron-probe microanalysis values.²⁴⁻²⁷ The samples were stored and transported in sealed containers filled with inert gas.

Sample preparation was done quickly in air within about 5 min to minimize uncontrolled environmental exposure which can induce an increase of T_c .^{12,28} We started sample

preparation by cleaving slabs from the inner part of the crystals with a typical thickness of 50–100 μm . The slabs had shiny cleavage surfaces and were further cut into smaller pieces for TDR (typically $0.5 \times 0.5 \text{ mm}^2$) and resistivity measurements. Cleaved internal parts of single crystals did not show any visible reaction with air and turned out to be relatively stable, contrary to crystals with the residue of NaAs flux, which aggressively reacts with air and moisture. After preparation, samples were promptly measured and immediately stored after measurements in an inert and dry environment. After each dipper run samples were washed with toluene to remove remaining Apiezon N grease in order to control the air exposure.

Samples for in-plane resistivity measurements had typical dimensions of $(1\text{--}2) \times 0.5 \times (0.02\text{--}0.1) \text{ mm}^3$. All sample dimensions were measured with an optical microscope with an accuracy of about 10%. Sample resistivity at room temperature, $\rho(300 \text{ K})$, was in the range 400–500 $\mu\Omega \text{ cm}$ for all compositions studied. This value is obtained on a bigger array of samples than in our previous study¹² and is somewhat higher. It is also somewhat higher than values found in electron-^{6,29} and hole-doped¹⁰ Ba122 compounds, typically 300 $\mu\Omega \text{ cm}$ or less. We do not have a sufficient array of data to obtain lower error bars needed to resolve the doping evolution of $\rho(300 \text{ K})$, if any exists. Contacts for four-probe resistivity measurements were made by soldering 50- μm silver wires with ultrapure Sn solder, as described in Ref. 30. Resistivity measurements were performed in *Quantum Design* physical property measurement system (PPMS), providing magnetic fields up to 9 T. For measurements of the upper critical field, H_{c2} , samples were glued to the side of a plastic block with the *ab* plane of the sample oriented to be either parallel or perpendicular to the direction of magnetic field (with an accuracy of about 1°).

Interplane resistivity measurements were done using the two-probe technique, relying on very low contact resistance of soldered contacts, typically in the 10- $\mu\Omega$ range. The top and bottom surfaces of the *ab* plane (typically $0.5 \times 0.5 \text{ mm}^2$ area) of the samples were covered with Sn solder forming a capacitorlike structure. A four-probe scheme was used to measure a sample with contacts, giving a sum of series connected sample, R_s , and contact, R_c , resistances. Since $R_s \gg R_c$, contact resistance represents a minor portion, on the order of 1–5% of the total resistance. This can be directly seen for our samples for temperatures below the superconducting T_c , where $R_s = 0$ and the measured resistance represents R_c .^{4,30,31} Further details of the measurement procedure can be found in Refs. 4–6.

The drawback of the measurement of samples with $c \ll a$ is that any structural and chemical inhomogeneity along the *c* axis, a very common problem in soft and micaceous samples of iron arsenide superconductors,^{4,32,33} not only increases sample resistance, but admixes the in-plane component due to the redistribution of the current. One way to ascertain correctness of the ρ_c measurements is to rely on measurements with the lowest resistivity values. Typically the best results were obtained on the thinnest slabs. To get reliable results we performed measurements of ρ_c on at least five samples of each batch. In all cases we obtained qualitatively similar temperature dependencies of the normalized electrical resistivity,

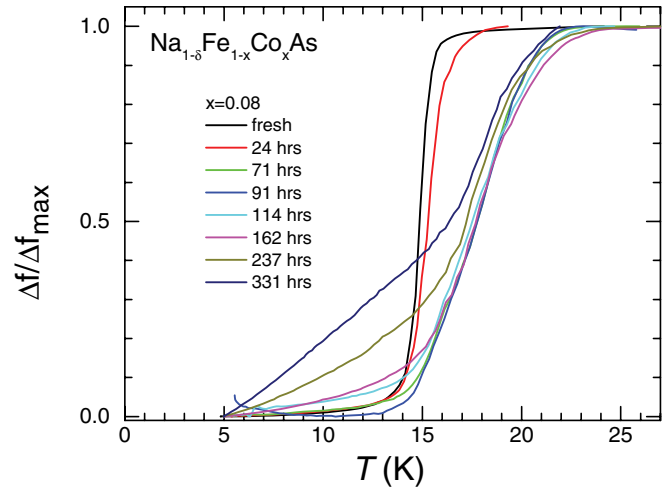


FIG. 1. (Color online) Evolution of the frequency shift signal in the dipper TDR experiment on increasing time of air-exposure treatment in crystals of slightly overdoped $\text{Na}_{1-\delta}\text{Fe}_{1-x}\text{Co}_x\text{As}$, $x = 0.08$. Similar to the parent compound (Ref. 12), T_c of the sample increases with exposure time to a maximum and then decreases. Similar effects are observed for other doping levels x .

$\rho_c(T)/\rho_c(300 \text{ K})$. The resistivity value at room temperature, $\rho_c(300 \text{ K})$, however, showed a notable scattering and was typically in the range 2000–3000 $\mu\Omega \text{ cm}$ at room temperature.

We have shown previously that reaction with air strongly affects the value of $\rho_a(300 \text{ K})$ due to the development of cracks.¹² Cracks grossly affect the internal sample connectivity and, hence, homogeneous current distribution, thus making interplane resistivity measurements of environmentally exposed samples impossible.

III. RESULTS

A. Environmental stability

The T_c of the parent $\text{Na}_{1-\delta}\text{FeAs}$ increases significantly upon exposure to air,^{12,34} water,²⁸ and Apiezon N grease.¹² Here, we study how the sensitivity of T_c to exposure changes with Co doping. In Fig. 1 we show the evolution of the TDR signal in slightly overdoped, $x = 0.08$ (fresh sample $T_c = 16 \text{ K}$), samples on exposure to air. Similar to the parent compound,¹² for all compositions irrespective of their x , the T_c of the samples increases initially upon air exposure and then decreases with prolonged exposure. The doping variation of TDR signal during fixed time, one-day air exposure, is summarized in Fig. 2. Variations of fresh sample T_c , highest achieved T_c during air exposure and fixed time (one-day) exposure as a function of x are summarized in Fig. 3.

One-day exposure of a sample to air does not lead to a visual appearance of reaction products. Thus, at least at this initial stage, there is no reason to assume transformation of NaFeAs into NaFe_2As_2 , the final product of reaction with water,²⁸ formed after a one-month exposure, which most likely shows up in Fig. 1 as a new shoulder in the temperature-dependent frequency shift at about 12 K for samples exposed for about two weeks.

In parent $\text{Na}_{1-\delta}\text{FeAs}$ the environmental reaction is caused by the variation of Na content in the samples, δ , due to

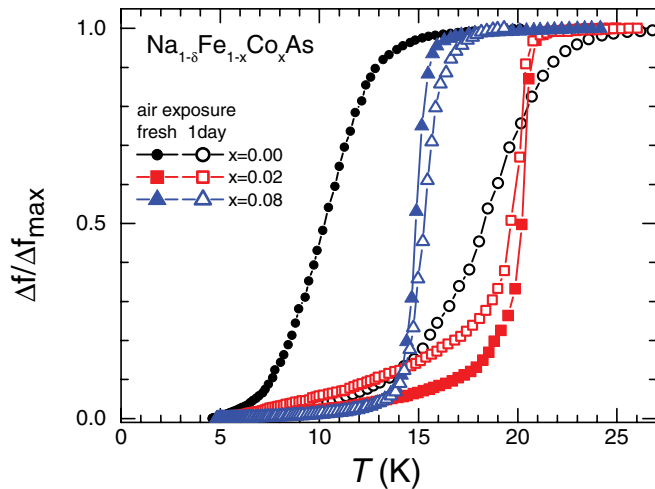


FIG. 2. (Color online) Doping evolution of the frequency shift signal in the dipper TDR experiment during fixed time air-exposure treatment of $\text{NaFe}_{1-x}\text{Co}_x\text{As}$ for 24 h. As can be seen, T_c increase from 12 to 22 K, characteristic of parent NaFeAs samples, is strongly suppressed with Co doping.

oxidative deintercalation.²⁸ It is natural to expect a similar effect in the Co-doped $\text{NaFe}_{1-x}\text{Co}_x\text{As}$. However, the puzzling observation is that T_c increases for both environmental reaction in pure $\text{Na}_{1-\delta}\text{FeAs}$ (presumably holelike doping) and electron Co doping. As such, it is not clear if carrier type and density change is the main effect involved. We note that detailed study of the effect of Li deficiency in a closely related LiFeAs superconductor found suppression of T_c , but virtually no change in the normal-state properties.³⁵ If Na deficiency leads to the formation of Na vacancies, this should lead to hole doping and, thus, move the dome on the doping phase diagram in an opposite way to electron Co doping. Further studies are required to understand what type of doping is induced by the loss of Na and what types of defects are formed.

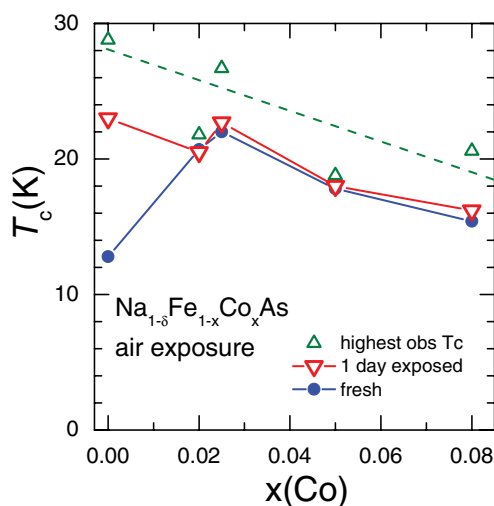


FIG. 3. (Color online) Doping evolution of the superconducting T_c in the dipper TDR experiment during air-exposure treatment of $\text{NaFe}_{1-x}\text{Co}_x\text{As}$. Blue solid dots show T_c of fresh samples, red down triangles T_c of the samples exposed to air for one day. Green up triangles show maximum onset T_c obtained in these experiments.

At a first glance, the different rate of T_c variation in Fig. 3 can be attributed to the different sensitivity of $T_c(x)$ in different parts of the phase diagram, being smallest at the flat optimal doping region. Indeed, the slope of $T_c(x)$ changes from very high for the parent compound to negligible in samples close to optimal doping. However, we find a rise in T_c after environmental reaction even in overdoped samples. This contradicts the simple relation of the rate of T_c change to be determined by a position on the phase diagram. Recently it was found that application of moderate pressure increases T_c for $\text{NaFe}_{1-x}\text{Co}_x\text{As}$ even in the overdoped regime,²⁶ which is similar to the response of T_c to environmental exposure; see Figs. 2 and 3. This fact may be suggestive that the increase in the internal strain might be playing some role in the initial increase of T_c in environmentally exposed samples. Our observations are also in agreement with the report that Co doping increases the stability of the samples.²⁴

B. Resistivity measurements

The temperature-dependent resistivity of “fresh” crystals of $\text{NaFe}_{1-x}\text{Co}_x\text{As}$ is shown in Fig. 4 using a normalized resistivity scale, $\rho/\rho(300\text{ K})$. The shape of $\rho_a(T)$ in the parent compound is relatively complex, with features due to split structural (at temperature $T_s = 55\text{ K}$) and magnetic (at $T_m = 45\text{ K}$) transitions^{19,36} and slope changes at higher temperatures.^{12,37} With doping the dependence transforms to very close to T -linear $\rho_a(T)$ in samples with $x = 0.08$ and close to T^2 on further x increase. The changes of slope at $T_1 \sim 300\text{ K}$ (increase of slope on cooling), $T_2 \sim 160\text{ K}$ (decrease of slope on cooling), and $T_3 \sim 80\text{ K}$ (increase of slope on cooling) are observed in doped samples, similar to the parent compound, and are relatively insensitive to doping. The feature at T_1 is observed in samples with all x studied. It is similar, though less pronounced, to a slope change at about the same temperature in $\rho_a(T)$ of stoichiometric LiFeAs , Refs. 38 and 39; see Fig. 4.

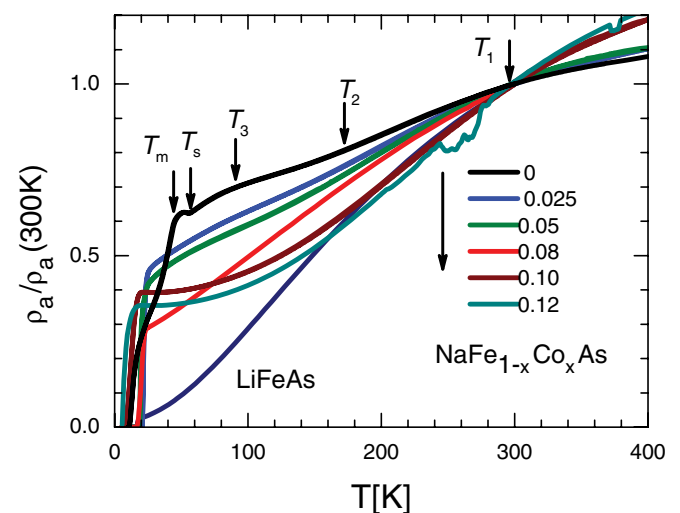


FIG. 4. (Color online) Doping evolution of the temperature dependence of the in-plane resistivity, $\rho_a/\rho_a(300\text{ K})$, for samples of $\text{NaFe}_{1-x}\text{Co}_x\text{As}$ in fresh state after initial sample handling and contact making. For reference we show data from Refs. 38 and 39 for stoichiometric LiFeAs , representative of the overdoped regime.

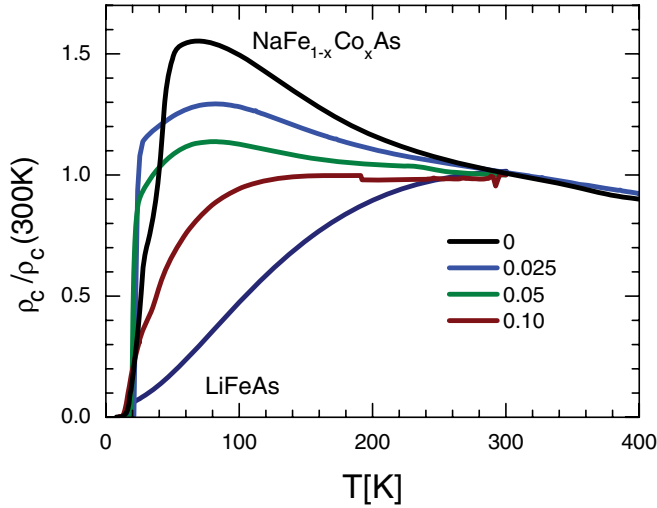


FIG. 5. (Color online) Doping evolution of the temperature dependence of the interplane resistivity, $\rho_c/\rho_c(300\text{ K})$, for samples of $\text{NaFe}_{1-x}\text{Co}_x\text{As}$ in fresh state after initial sample handling and contact making. For reference we show data from Refs. 38 and 39 for stoichiometric LiFeAs , representative of the overdoped regime.

The features at T_2 and T_3 are observed in $\rho_a(T)$ of the samples with $x \leq 0.05$.

The results of this study of $\rho_a(T)$ are in reasonable agreement with previous studies on single crystals,^{24,37} with the difference of x coming from using nominal values during sample preparation. The doping transformation of the temperature dependent resistivity for T right above T_c follows general expectations for a quantum critical scenario,⁹ with T -linear range confined from the high-temperature side by slope change on approaching T_1 . By comparison with

position of maximum in the temperature-dependent interplane resistivity $\rho_c(T)$, we assigned a similar slope change feature in $\rho_a(T)$ of $\text{Ba}_{1-x}\text{K}_x\text{Fe}_2\text{As}_2$ to formation of pseudogap.¹³ The slope changes upon cooling through T_2 and T_3 in samples with $x \leq 0.05$ do not have a direct analogy with Ba122 compounds. These features are observed even in samples in which long-range magnetic order and orthorhombic structural distortion are suppressed. Studies of resistivity anisotropy on detwinned single crystals of parent NaFeAs (Refs. 27 and 37) suggest that the feature at T_3 has a similar nature to nematic correlations, which is particularly strong in electron-doped BaCo122 .^{16,17}

For understanding the resistivity of NaFeAs -based compounds, it is important to get insight into the temperature dependence of the interplane resistivity component. In Fig. 5 we show the doping evolution of $\rho_c(T)$ in $\text{NaFe}_{1-x}\text{Co}_x\text{As}$. The interplane resistivity of parent NaFeAs increases during cooling down to a rounded maximum at ~ 70 K, which is close to T_3 as determined from $\rho_a(T)$. The resistivity rapidly decreases below this maximum, with a notable rate increase below T_m . Note that contrary to $\rho_a(T)$, the interplane resistivity does not show an increase below T_s , suggesting that the carriers affected by the formation of a gap do not contribute much to the interplane transport. Interestingly, despite the strong difference between $\rho_a(T)$ and $\rho_c(T)$, the high-temperature features are observed in both of them.

C. Anisotropy of the upper critical field

The anisotropy of the electrical resistivity at T_c , $\gamma_\rho \equiv \frac{\rho_c(T_c)}{\rho_a(T_c)}$, is linked with the anisotropy of the upper critical field, $\gamma_H \equiv \frac{H_{c2,ab}(T_c)}{H_{c2,c}(T_c)}$, with $\gamma_\rho = \gamma_H^2$. Because determination of the absolute values in resistivity measurements always

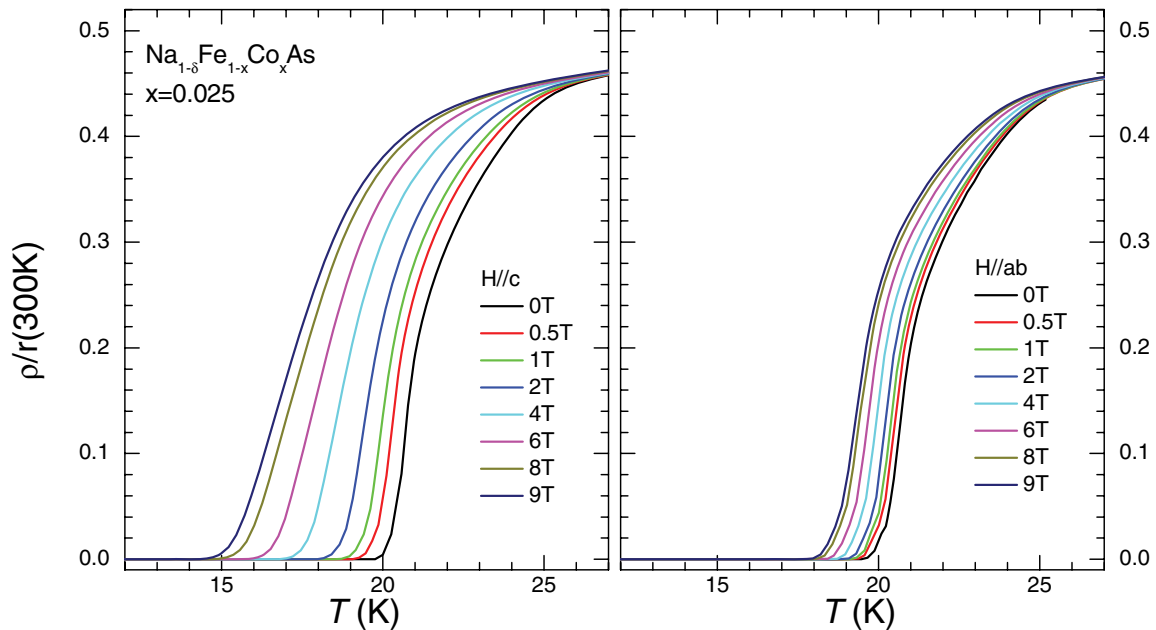


FIG. 6. (Color online) Evolution of the temperature-dependent resistivity in the vicinity of the superconducting transition in magnetic fields applied perpendicular to ($H \parallel c$, left panel) and parallel to ($H \parallel ab$, right panel) the conducting Fe-As plane of the sample of optimally doped $\text{NaFe}_{1-x}\text{Co}_x\text{As}$, $x = 0.025$. The resistive transition temperature, used to plot H - T phase diagram shown in Fig. 7 below, was defined using midpoint criterion.

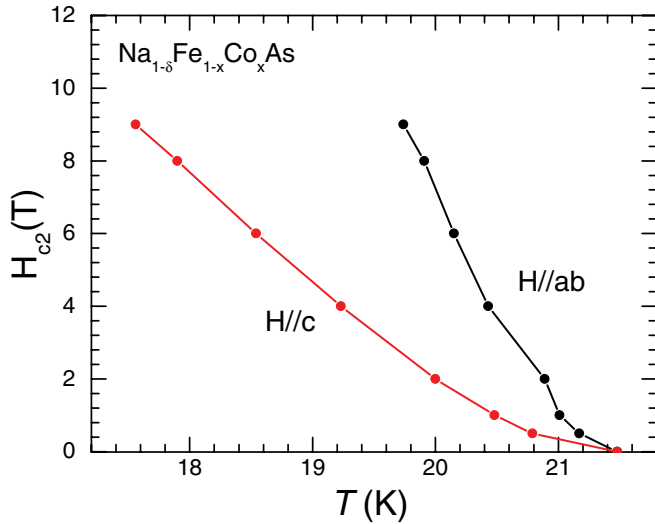


FIG. 7. (Color online) Temperature and magnetic-field phase diagram of optimally doped $\text{NaFe}_{1-x}\text{Co}_x\text{As}$, $x = 0.025$ for orientation of magnetic field perpendicular and parallel to the conducting Fe-As plane of the crystal.

includes uncertainty of the geometric factor and is affected by the cracks, the H_{c2} anisotropy measurements provide an alternative way to evaluate resistivity anisotropy.⁴ In Fig. 6 we zoom the superconducting transition in in-plane resistivity measurements $\rho_a(T)$ for a sample with doping level close to optimal, $x = 0.025$. The same sample was remounted on a plastic cube with the magnetic field in the $H \parallel c$ (left panel) and $H \parallel ab$ (right panel) configurations.

We used the resistive transition midpoint to determine $H_{c2}(T)$ anisotropy as shown in Fig. 7. Close to T_c the anisotropy $\gamma_H = 2.25 \pm 0.1$ for the sample with $x = 0.025$. Similar value with $\gamma_H = 2.35 \pm 0.1$ was obtained in sample with $x = 0.08$. These measurements suggest a resistivity anisotropy of about 5 at T_c . Considering that $\gamma_\rho(T_c) \sim 2\gamma_\rho(300\text{ K})$ (see Figs. 4 and 5) we expect a negligible anisotropy of 2–3 at room temperature. The direct resistivity measurements, with $\rho_a(300\text{ K}) = 400\text{--}500\ \mu\Omega\text{ cm}$ and $\rho_c(300\text{ K}) = 2000\text{--}3000\ \mu\Omega\text{ cm}$, suggest an anisotropy of 4–8. The origin of this factor of about 2 discrepancy remains unclear at the moment.

IV. DISCUSSION

A. Slope-change features in the temperature-dependent resistivity

As can be seen from direct comparison of in-plane and interplane resistivity in the parent and slightly doped $x = 0.025$ compositions, Fig. 8, features in $\rho_a(T)$ find counterparts in $\rho_c(T)$. For example, a slope decrease in generally metallic $\rho_a(T)$ below $T_2 \sim 160\text{ K}$ is seen as slope increase in generally activated (increasing on cooling) $\rho_c(T)$. This similarity found in two very different dependencies suggests that the activation of carriers over a partial gap, rather than change of scattering, is responsible for the feature. Partial (nematic) order,^{27,37} which happens above the structural transition at T_3 , changes $\rho_c(T)$ from insulating to metallic, while the magnetic order below T_m causes a dramatic decrease of resistivity in both directions

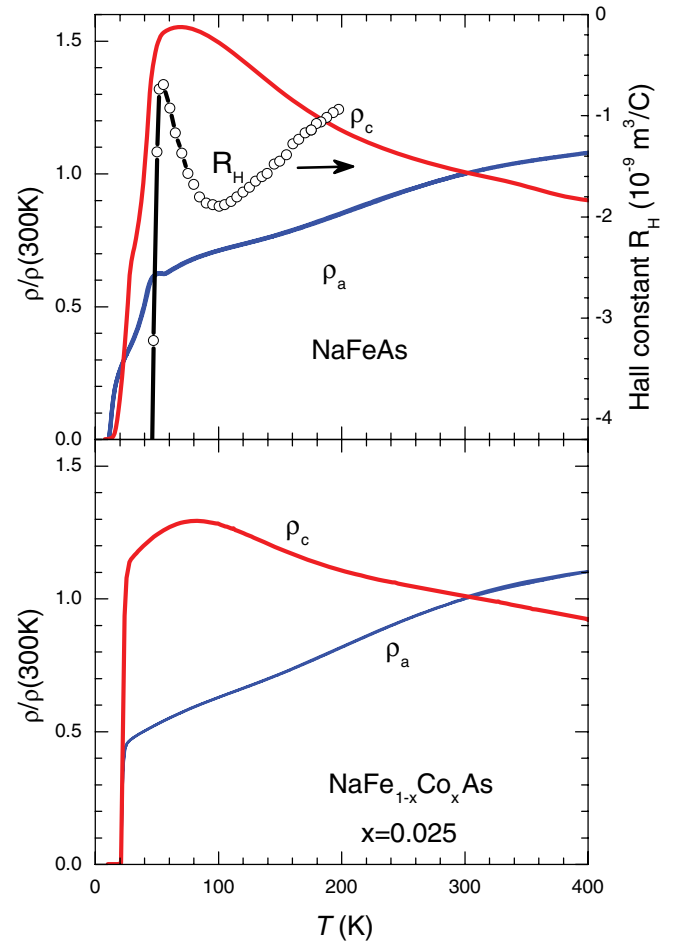


FIG. 8. (Color online) Top panel: Comparison of the temperature-dependent in-plane and interplane resistivities of parent NaFeAs . For reference we show temperature-dependent Hall constant $R_H(T)$, right scale, with the data taken from Ref. 27. Bottom panel: Comparison of in-plane and interplane resistivities in a sample with $x = 0.025$. The data are plotted on a normalized scale, $\rho(T)/\rho(300\text{ K})$.

of charge flow. The decrease is especially strong in the parent compound in which the residual resistivity ratio (RRR), $\rho(300\text{ K})/\rho(T_c)$, is a factor of 2 higher than in $x = 0.025$. These observations suggest that magnetic scattering plays an important role in resistivity at $T > T_3$, and that, when inelastic scattering is dominant (as in the parent compound), taming down of magnetic fluctuations reveals intrinsically very low residual resistivity.

Interestingly, the position of the broad crossover maximum in $\rho_a(T)$ and $\rho_c(T)$ as a function of temperature roughly corresponds to the minimum in the temperature dependence of the Hall coefficient $R_H(T)$; see the top panel in Fig. 8 (the data for $R_H(T)$ were taken from Ref. 27). Similarly, the evolution of these features can be traced together with the composition x in $\text{NaFe}_{1-x}\text{Co}_x\text{As}$.²⁷

B. Residual resistivity

Observation of a much higher RRR in nondoped materials agrees with studies in Ba122 compounds, though in the latter, the direct comparison is not so simple. In the case of NaFeAs -based materials we can compare the RRR of

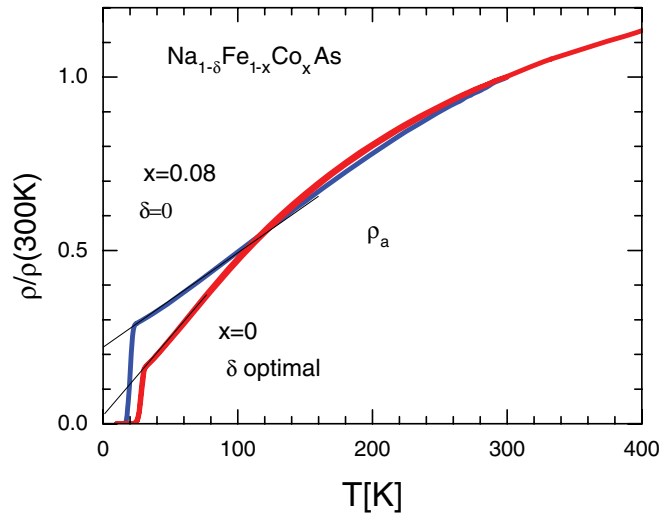


FIG. 9. (Color online) Comparison of the temperature-dependent in-plane resistivity in samples of NaFeAs doped to the highest T_c by environmental reaction with Apiezon N grease and with Co doping, $x = 0.05$. Resistivity data are plotted vs normalized scale, $\rho(T)/\rho(300\text{ K})$. Lines show linear extrapolation of the curves to $T \rightarrow 0$, revealing difference in residual resistivity of two concentrations of samples.

the samples, brought to optimal doping using two different ways of doping, electron with Co substitution of Fe and environmental, on interaction with the environment. In Fig. 9 we compare T -dependent resistivity in two representative samples, extrapolating curves linearly from T_c to $T = 0$. The RRR ratio decreases from more than 20 in environmentally doped samples to about 4 in Co-doped samples. Taking that resistivity at room temperature does not change from about

$400\ \mu\Omega\text{ cm}$; this suggests that the residual resistivity induced by the $x = 0.025$ substitution of Fe atoms with Co is on the order of $100\ \mu\Omega\text{ cm}$, comparable to BaCo122.⁶ This is almost a factor of 5 higher than the value found in very disordered samples, doped with environmental reaction, which extrapolates to $\rho_0 \approx 20\ \mu\Omega\text{ cm}$.

V. CONCLUSIONS

In conclusion, we find that the complicated shape of the temperature-dependent interplane resistivity of both parent NaFeAs and Co-doped $\text{NaFe}_{1-x}\text{Co}_x\text{As}$ shows the same anomalies as in-plane resistivity. This is particularly interesting considering the fact that interplane transport is clearly thermally activated, while the in-plane resistivity follows metallic decrease on cooling. This finding suggests that the observed features are not caused by a particular type of scattering process and most likely are determined by the variation in the carrier density. Such behavior strongly supports the idea that these features are caused by the thermal activation of charge carriers over the pseudogap in the electronic spectrum. This conclusion suggests that the pseudogap is a common feature of both NaFeAs-based materials and BaFe_2As_2 -derived compounds.^{6,7,40}

ACKNOWLEDGMENTS

We thank Seyeon Park for her help with dipper measurements. Work at the Ames Laboratory was supported by the Department of Energy Basic Energy Sciences under Contract No. DE-AC02-07CH11358. The single-crystal growth effort at UT was supported by US DOE BES under Grant No. DE-FG02-05ER46202 (P.D.).

*Corresponding author: tanatar@ameslab.gov

†prozorov@ameslab.gov

¹J. Paglione and R. L. Greene, *Nature Phys.* **6**, 645 (2010).

²D. C. Johnston, *Adv. Phys.* **59**, 803 (2010).

³G. R. Stewart, *Rev. Mod. Phys.* **83**, 1589 (2011).

⁴M. A. Tanatar, N. Ni, C. Martin, R. T. Gordon, H. Kim, V. G. Kogan, G. D. Samolyuk, S. L. Bud'ko, P. C. Canfield, and R. Prozorov, *Phys. Rev. B* **79**, 094507 (2009).

⁵M. A. Tanatar, N. Ni, G. D. Samolyuk, S. L. Bud'ko, P. C. Canfield, and R. Prozorov, *Phys. Rev. B* **79**, 134528 (2009).

⁶M. A. Tanatar, N. Ni, A. Thaler, S. L. Bud'ko, P. C. Canfield, and R. Prozorov, *Phys. Rev. B* **82**, 134528 (2010).

⁷M. A. Tanatar, N. Ni, A. Thaler, S. L. Bud'ko, P. C. Canfield, and R. Prozorov, *Phys. Rev. B* **84**, 014519 (2011).

⁸See, for example, N. Hussey, *J. Phys.: Condens. Matter* **20**, 123201 (2008).

⁹N. Doiron-Leyraud, P. Auban-Senzier, S. René de Cotret, C. Bourbonnais, D. Jérôme, K. Bechgaard, and L. Taillefer, *Phys. Rev. B* **80**, 214531 (2009).

¹⁰B. Shen, H. Yang, Z.-S. Wang, F. Han, B. Zeng, L. Shan, C. Ren, and H.-H. Wen, *Phys. Rev. B* **84**, 184512 (2011).

¹¹S. Kasahara, T. Shibauchi, K. Hashimoto, K. Ikada, S. Tonegawa, R. Okazaki, H. Shishido, H. Ikeda, H. Takeya, K. Hirata, T. Terashima, and Y. Matsuda, *Phys. Rev. B* **81**, 184519 (2010).

¹²M. A. Tanatar, N. Spyrison, K. Cho, E. C. Blomberg, G. Tan, P. Dai, C. Zhang, and R. Prozorov, *Phys. Rev. B* **85**, 014510 (2012).

¹³M. A. Tanatar, E. C. Blomberg, H. Kim, K. Cho, W. E. Straszheim, B. Shen, H.-H. Wen, and R. Prozorov, *arXiv:1106.0533*.

¹⁴L. Taillefer, *Annu. Rev. Condens. Matter Phys.* **1**, 51 (2010).

¹⁵R. M. Fernandes, A. V. Chubukov, J. Knolle, I. Eremin, and J. Schmalian, *Phys. Rev. B* **85**, 024534 (2012).

¹⁶J.-H. Chu, J. G. Analytis, K. De Greve, P. L. McMahon, Z. Islam, Y. Yamamoto, and I. R. Fisher, *Science* **329**, 824 (2010).

¹⁷M. A. Tanatar, E. C. Blomberg, A. Kreyssig, M. G. Kim, N. Ni, A. Thaler, S. L. Bud'ko, P. C. Canfield, A. I. Goldman, I. I. Mazin, and R. Prozorov, *Phys. Rev. B* **81**, 184508 (2010).

¹⁸E. C. Blomberg, M. A. Tanatar, R. M. Fernandes, B. Shen, H.-H. Wen, J. Schmalian, and R. Prozorov, *arXiv:1202.4430*.

¹⁹D. R. Parker, M. J. P. Smith, T. Lancaster, A. J. Steele, I. Franke, P. J. Baker, F. L. Pratt, M. J. Pitcher, S. J. Blundell, and S. J. Clarke, *Phys. Rev. Lett.* **104**, 057004 (2010).

²⁰J. D. Wright, T. Lancaster, I. Franke, A. J. Steele, J. S. Möller, M. J. Pitcher, A. J. Corkett, D. R. Parker, D. G. Free, F. L. Pratt, P. J. Baker, S. J. Clarke, and S. J. Blundell, *Phys. Rev. B* **85**, 054503 (2012).

²¹C. T. Vandegrift, *Rev. Sci. Instrum.* **46**, 599 (1975).

²²R. Prozorov, R. W. Giannetta, A. Carrington, and F. M. Araujo-Moreira, *Phys. Rev. B* **62**, 115 (2000).

- ²³C. He, Y. Zhang, B. P. Xie, X. F. Wang, L. X. Yang, B. Zhou, F. Chen, M. Arita, K. Shimada, H. Namatame, M. Taniguchi, X. H. Chen, J. P. Hu, and D. L. Feng, *Phys. Rev. Lett.* **105**, 117002 (2010).
- ²⁴A. F. Wang, X. G. Luo, Y. J. Yan, J. J. Ying, Z. J. Xiang, G. J. Ye, P. Cheng, Z. Y. Li, W. J. Hu, and X. H. Chen, *Phys. Rev. B* **85**, 224521 (2012).
- ²⁵S. Y. Zhou, X. C. Hong, X. Qiu, B. Y. Pan, Z. Zhang, X. L. Li, W. N. Dong, A. F. Wang, X. G. Luo, X. H. Chen, and S. Y. Li, [arXiv:1204.3440](https://arxiv.org/abs/1204.3440).
- ²⁶A. F. Wang, Z. J. Xiang, J. J. Ying, Y. J. Yan, P. Cheng, G. J. Ye, X. G. Luo, and X. H. Chen, [arXiv:1207.5382](https://arxiv.org/abs/1207.5382).
- ²⁷A. F. Wang, J. J. Ying, X. G. Luo, Y. J. Yan, D. Y. Liu, Z. J. Xiang, P. Cheng, G. J. Ye, L. J. Zou, Z. Sun, and X. H. Chen, [arXiv:1207.3852](https://arxiv.org/abs/1207.3852).
- ²⁸I. Todorov, D. Y. Chung, H. Claus, C. D. Malliakas, A. P. Douvalis, T. Bakas, J. Q. He, V. P. Dravid, and M. G. Kanatzidis, *Chem. Mater.* **22**, 3916 (2010).
- ²⁹F. Rullier-Albenque, D. Colson, A. Forget, and H. Alloul, *Phys. Rev. Lett.* **103**, 057001 (2009).
- ³⁰M. A. Tanatar, N. Ni, S. L. Bud'ko, P. C. Canfield, and R. Prozorov, *Supercond. Sci. Technol.* **23**, 054002 (2010).
- ³¹R. Prozorov, N. Ni, M. A. Tanatar, V. G. Kogan, R. T. Gordon, C. Martin, E. C. Blomberg, P. Prommapan, J. Q. Yan, S. L. Bud'ko, and P. C. Canfield, *Phys. Rev. B* **78**, 224506 (2008).
- ³²N. Ni, M. E. Tillman, J.-Q. Yan, A. Kracher, S. T. Hannahs, S. L. Bud'ko, and P. C. Canfield, *Phys. Rev. B* **78**, 214515 (2008).
- ³³J. S. Bobowski, J. C. Baglo, J. Day, P. Dosanjh, R. Ofer, B. J. Ramshaw, R. Liang, D. A. Bonn, W. N. Hardy, H. Luo, Z.-S. Wang, L. Fang, and H.-H. Wen, *Phys. Rev. B* **82**, 094520 (2010).
- ³⁴K. Sasmal, B. Lv, Z. J. Tang, F. Chen, Y. Y. Xue, B. Lorenz, A. M. Guloy, and C. W. Chu, *Phys. Rev. B* **79**, 184516 (2009).
- ³⁵M. Wang, M. Wang, H. Miao, S. V. Carr, D. L. Abernathy, M. B. Stone, X. C. Wang, L. Xing, C. Q. Jin, X. Zhang, J. Hu, T. Xiang, H. Ding, and P. Dai, *Phys. Rev. B* **86**, 144511 (2012).
- ³⁶S. Li, C. de la Cruz, Q. Huang, G. F. Chen, T.-L. Xia, J. L. Luo, N. L. Wang, and P. Dai, *Phys. Rev. B* **80**, 020504 (2009).
- ³⁷Y. Zhang, C. He, Z. R. Ye, J. Jiang, F. Chen, M. Xu, Q. Q. Ge, B. P. Xie, J. Wei, M. Aeschlimann, X. Y. Cui, M. Shi, J. P. Hu, and D. L. Feng, *Phys. Rev. B* **85**, 085121 (2012).
- ³⁸Y. J. Song, J. S. Ghim, B. H. Min, Y. S. Kwon, M. H. Jung, and J.-S. Rhyee, *Appl. Phys. Lett.* **96**, 212508 (2010).
- ³⁹M. A. Tanatar, J.-Ph. Reid, S. Rene de Cotret, N. Doiron-Leyraud, F. Laliberte, E. Hassinger, J. Chang, H. Kim, K. Cho, Y. J. Song, Y. S. Kwon, R. Prozorov, and L. Taillefer, *Phys. Rev. B* **84**, 054507 (2011).
- ⁴⁰S. J. Moon, A. A. Schafgans, S. Kasahara, T. Shibauchi, T. Terashima, Y. Matsuda, M. A. Tanatar, R. Prozorov, A. Thaler, P. C. Canfield, A. S. Sefat, D. Mandrus, and D. N. Basov, *Phys. Rev. Lett.* **109**, 027006 (2012).